nature materials

LETTERS

PUBLISHED ONLINE: 16 JUNE 2013 | DOI: 10.1038/NMAT3675

Current-driven dynamics of chiral ferromagnetic domain walls

Satoru Emori[1], Uwe Bauer[1], Sung-Min Ahn[1], Eduardo Martinez[2] and Geoffrey S. D. Beach[1]*

In most ferromagnets the magnetization rotates from one domain to the next with no preferred handedness. However, broken inversion symmetry can lift the chiral degeneracy, leading to topologically rich spin textures such as spin spirals[1,2] and skyrmions[3–5] through the Dzyaloshinskii–Moriya interaction[6] (DMI). Here we show that in ultrathin metallic ferromagnets sandwiched between a heavy metal and an oxide, the DMI stabilizes chiral domain walls[2,7] (DWs) whose spin texture enables extremely efficient current-driven motion[8–11]. We show that spin torque from the spin Hall effect[12–15] drives DWs in opposite directions in Pt/CoFe/MgO and Ta/CoFe/MgO, which can be explained only if the DWs assume a Néel configuration[7,16] with left-handed chirality. We directly confirm the DW chirality and rigidity by examining current-driven DW dynamics with magnetic fields applied perpendicular and parallel to the spin spiral. This work resolves the origin of controversial experimental results[10,17,18] and highlights a new path towards interfacial design of spintronic devices.

Current-controlled DW displacement underpins the operation of an emerging class of spintronic memory[19] and logic[20,21] devices. In out-of-plane magnetized ferromagnets sandwiched between an oxide and a heavy metal, current-induced DW motion is anomalously efficient[8–11]. This observation has been widely attributed to a Rashba effective field[17,22,23] that stabilizes Bloch DWs against deformation, permitting high-speed motion[10] through conventional spin-transfer torque[24] (STT). However, current-induced DW motion is absent in symmetric Pt/Co/Pt (refs 8,9, 11,25) stacks, and semiclassical transport calculations[25] suggest that the spin-polarized current in the ultrathin (<1 nm) Co is vanishingly small. Moreover, DWs in Pt/Co/oxide move against electron flow[8,10,11], contrary to the action of STT (ref. 24). Together, these results suggest that conventional STT contributes negligibly to DW dynamics in these ultrathin structures and that interfacial phenomena[26,27] are instead responsible.

The Rashba field lacks the correct symmetry to drive DWs directly[16,26,27], and the spin Hall effect (SHE) in the adjacent heavy metal has emerged as a possible alternative mechanism[12–16,27]. SHE-driven spin accumulation at the heavy-metal/ferromagnet interface generates a Slonczewski-like torque[16,26,27] strong enough to switch uniformly magnetized films[12–15,18]. However, the Bloch DWs expected in typical nanowire geometries[8–11,28] have their plane oriented perpendicular to the nanowire axis, in which case the Slonczewski-like torque vanishes[16]. This behaviour was recently confirmed in asymmetric Pt/Co/Pt stacks in which the SHE-induced torques from the Pt layers did not cancel completely[15]. In that case, current-assisted DW depinning was observed when an applied field rotated the DW plane towards the nanowire axis, but up–down and down–up DWs were driven in opposite directions and the current had no effect in the absence of the bias field. The SHE alone is therefore incapable of uniformly driving trains of DWs in devices, and is insufficient to explain the high spin-torque efficiencies and DW velocities observed in Pt/Co/oxide[8–11] without applied fields.

Here we characterize current-induced torques and DW dynamics in out-of-plane magnetized Pt/CoFe/MgO and Ta/CoFe/MgO stacks that are nominally identical except for the heavy-metal underlayers, whose spin Hall angles are large and of opposite sign[12–14]. By considering the symmetry of the measured current-induced torque along with the DW dynamics driven by this torque, we uniquely identify the DW configuration as Néel with a fixed chirality. Magnetostatics alone makes this configuration unstable and does not favour one chirality over the other, but the DMI has been theoretically shown to promote chiral Néel DWs (refs 2,7). By applying in-plane magnetic fields, we verify that the DW magnetization aligns rigidly along the nanowire axis, and that the DW spin spiral exhibits a global chirality common to both Pt/CoFe/MgO and Ta/CoFe/MgO. Current-driven DW motion in heavy-metal/ferromagnet/oxide structures is naturally explained by the combination of the SHE, which produces the sole current-induced torque, and the DMI, which stabilizes chiral DWs whose symmetry permits uniform motion with very high efficiency.

DW motion was characterized in 500-nm-wide, 40-μm-long nanowires overlaid with an orthogonal DW nucleation line and lateral contacts for current injection (Fig. 1a). We first examine the effect of current on the threshold field H_{prop} for DW propagation through the defect landscape. Measurements were performed as in ref. 11, by first nucleating a reversed domain with the Oersted field from a current pulse through the nucleation line and then sweeping an out-of-plane field H_z to drive the DW along the nanowire. DW motion was detected through the polar magneto-optical Kerr effect, with a ≈3 μm laser spot positioned at the midpoint of the nanowire. Comparing Fig. 1d,e, H_{prop} varies linearly with electron current density j_e, but DW propagation is hindered in the electron flow direction in Pt/CoFe/MgO and assisted along electron flow in Ta/CoFe/MgO. This remarkable difference, produced simply by changing the non-magnetic metal in contact with the ferromagnet, was independent of the sense of magnetization (up–down or down–up) across the DW. The magnitude of the spin-torque efficiency, taken as the slope of H_{prop} versus j_e, was 120 Oe per 10^{11} A m^{-2} for Pt/CoFe/MgO and 170 Oe per 10^{11} A m^{-2} for Ta/CoFe/MgO. These large efficiencies are comparable to those reported for Pt/Co/AlOx (refs 9,10) and Pt/Co/GdOx (ref. 11), suggesting that a universal mechanism governs current-driven DW motion in heavy-metal/ferromagnet/oxide.

[1]Department of Materials Science and Engineering, Massachusetts Institute of Technology, Cambridge, Massachusetts 02139, USA, [2]Dpto. Física Aplicada. Universidad de Salamanca, Plaza de los Caidos s/n E-38008, Salamanca, Spain. *e-mail: gbeach@mit.edu

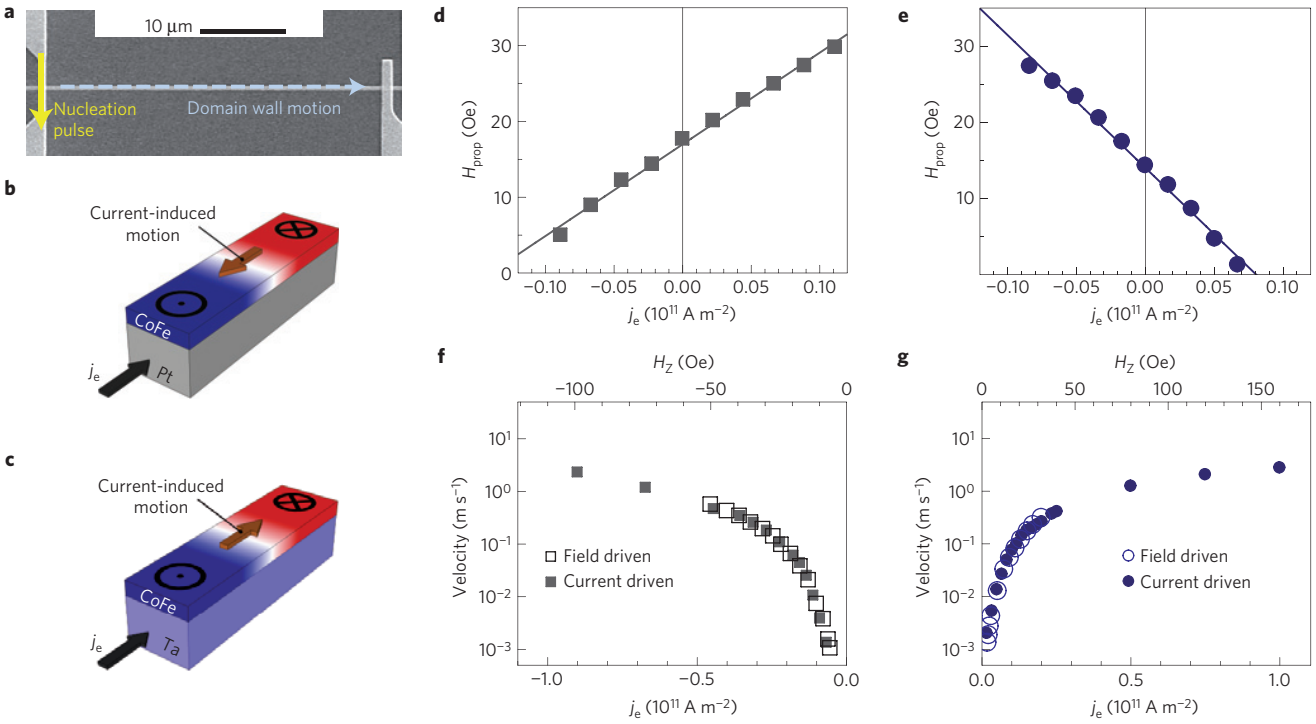

Figure 1 | Effect of current on DW motion. a, Scanning electron micrograph of the nanowire. The current pulse on the left nucleates a DW, which is then propagated to the right by current or applied out-of-plane field. **b**,**c**, Illustrations of the direction of current-driven DW motion in the Pt/CoFe/MgO (**b**) and Ta/CoFe/MgO (**c**) nanowires. Electron current j_e is defined positive when conduction electrons flow away from the nucleation line, from left to right in the micrograph (**a**). **d**,**e**, DW propagation field H_{prop} as a function of driving electron current density j_e for Pt/CoFe/MgO (**d**) and Ta/CoFe/MgO (**e**). The slope of the linear fit extracts the spin-torque efficiency for each structure. **f**,**g**, DW velocity as a function of j_e and applied out-of-plane field H_z for Pt/CoFe/MgO (**f**) and Ta/CoFe/MgO (**g**). The field-driven data are scaled by a field-to-current ratio (see text) so that they are directly on top of the current-driven data.

In Fig. 1f,g, we directly compare field-driven and current-driven DW velocities, measured using a time-of-flight technique[11]. Again, DWs moved against electron flow in Pt/CoFe/MgO (Fig. 1f) and along electron flow in Ta/CoFe/MgO (Fig. 1g). The maximum field was limited by random domain nucleation, and the exponential dependence of velocity on H_z and j_e indicates thermally activated motion[11,29]. The field-driven and current-driven velocities exhibit the same dynamical scaling across three decades in velocity when j_e is scaled by a constant (110 Oe per 10^{11} A m^{-2} for Pt/CoFe/MgO and 160 Oe per 10^{11} A m^{-2} for Ta/CoFe/MgO). These field-to-current ratios closely match those extracted from Fig. 1d,e. We therefore conclude that the effect of current on DW motion is phenomenologically equivalent to an out-of-plane field[9,11], which reveals the symmetry of the current-induced torque as discussed later.

In addition to robust DW motion, current enables switching between uniformly magnetized up and down states with the assistance of a constant in-plane magnetic field[12,15,18]. This switching phenomenon was demonstrated in 1,200-nm-wide Hall crosses (Fig. 2a). A sequence of 250-ms-long current pulses with increasing (or decreasing) amplitude was injected along the x axis, and in between each pulse the out-of-plane magnetization component M_z was measured from the anomalous Hall voltage using a low-amplitude ($\sim 10^9$ A m^{-2}) a.c. sense current and a lock-in amplifier. Figure 2d,e plots M_z versus j_e, under a constant applied longitudinal field H_L. This field tilted the magnetization away from the z axis by $\approx 5°$ in Pt/CoFe/MgO at 500 Oe and $\approx 3°$ in Ta/CoFe/MgO at 100 Oe, but did not bias M_z up or down, as evidenced by the nearly symmetric switching profile (Fig. 2d,e). With sufficiently large H_L and j_e in the $+x$ direction, the up magnetized state was favoured in Pt/CoFe/MgO (Fig. 2d, solid line), whereas the down state was favoured in Ta/CoFe/MgO (Fig. 2e, solid line). When the direction of H_L or j_e was reversed, the preferred magnetization direction was also reversed (Fig. 2d,e, dotted lines).

This switching behaviour implies that j_e generates an effective field $\mathbf{H}_{SL}$ associated with a Slonczewski-like torque[12,13,15,18], given by $\mathbf{H}_{SL} = H_{SL}^0(\hat{m} \times (\hat{z} \times \hat{j}_e))$ (ref. 16). Here $\hat{m}$, $\hat{z}$ and $\hat{j}_e$ are unit vectors along the magnetization, z axis and electron flow, respectively, and H_{SL}^0 parameterizes the torque. The SHE in the heavy metal directly generates a Slonczewski-like torque, but the Rashba effect can also yield a torque of this form due to spin relaxation[18,26,27]. Assuming the SHE is the dominant source, justified experimentally below, H_{SL}^0 is related to the spin Hall angle θ_{SH} in the heavy metal through $H_{SL}^0 = \hbar\theta_{SH}|j_e||/(2|e|M_S t_F)$ (ref. 16), with M_S being the saturation magnetization and t_F the ferromagnet thickness. From the sign of H_{SL}^0 extracted from current-induced switching (Fig. 2b,c), θ_{SH} is positive in Pt and negative in Ta, consistent with refs 12,13.

We quantified the Slonczewski-like torque by detecting magnetization tilting induced by a.c. current using the anomalous Hall voltage as described in refs 22,30 (see Supplementary Information). The scaling of H_{SL} with current is shown in Fig. 3. When the magnetization was up and j_e was in the $+x$ direction, H_{SL} pointed along $-x$ in Pt/CoFe/MgO (Fig. 3a,e) and $+x$ in Ta/CoFe/MgO (Fig. 3b,f), in agreement with our analysis of magnetization switching (Fig. 2b,c). The direction of H_{SL} reversed when the magnetization was oriented down. The linear fit in Fig. 3a reveals a large H_{SL}^0 in Pt/CoFe/MgO of magnitude 50 Oe per 10^{11} A m^{-2}, implying $\theta_{SH} = +0.06$ in Pt, which agrees well with ref. 12. The magnitude of H_{SL}^0 in Ta/CoFe/MgO is ≈ 200 Oe per 10^{11} A m^{-2}, implying $\theta_{SH} = -0.25$ in Ta, twice as large as in ref. 13 and closer to the value reported for W (ref. 14).

The current-induced effective transverse field H_{FL}, often associated with a field-like torque from the Rashba effect[16,17,22,23,26,27], was quantified similarly[22,30] (see Supplementary Information). Unlike H_{SL}, the direction of H_{FL} was independent of the magnetization

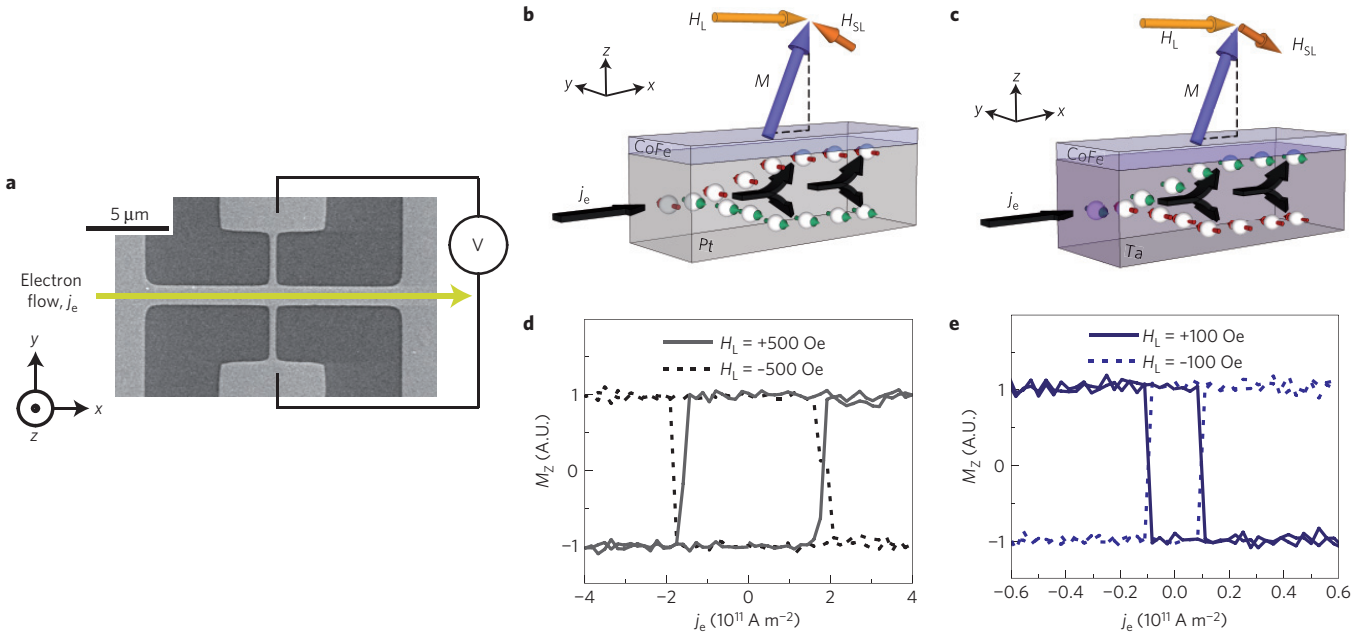

Figure 2 | Current-induced switching under a constant in-plane longitudinal field. a, Scanning electron micrograph of a Hall cross. **b**,**c**, Illustrations of Pt/CoFe/MgO (**b**) and Ta/CoFe/MgO (**c**) in the up magnetization state with the injected electron current and applied longitudinal field H_L in the $+x$ direction. Owing to the combination of the current-induced Slonczewski-like torque (producing an effective field H_{SL}) and the applied longitudinal field, up magnetization is stable in Pt/CoFe/MgO whereas it is unstable in Ta/CoFe/MgO. **d**,**e**, Out-of-plane magnetization M_z (normalized anomalous Hall signal) as a function of electron current density j_e under a constant H_L in Pt/CoFe/MgO (**d**) and Ta/CoFe/MgO (**e**). The magnitude of H_L is 500 Oe for Pt/CoFe/MgO (**d**) and 100 Oe for Ta/CoFe/MgO (**e**). When H_L is reversed from $+x$ (solid line) to $-x$ (dotted line), the stable magnetization direction under a given current polarity reverses.

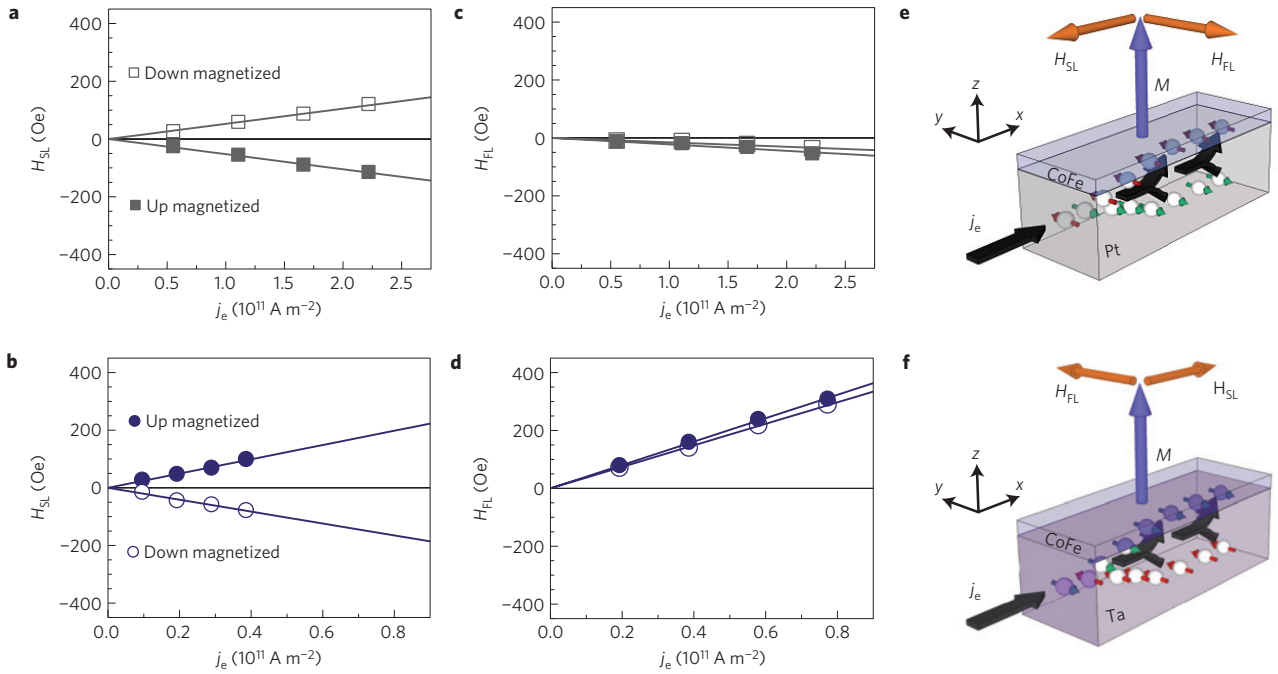

Figure 3 | Current-induced effective fields. a,**b**, Current-induced effective longitudinal field H_{SL}, arising directly from the Slonczewski-like torque, as a function of electron current density j_e (from a.c. excitation current amplitude) in Pt/CoFe/MgO (**a**) and Ta/CoFe/MgO (**b**). **c**,**d**, Current-induced effective transverse field H_{FL} as a function of j_e in Pt/CoFe/MgO (**c**) and Ta/CoFe/MgO (**d**). **e**,**f**, Illustration of the directions of the current-induced effective fields H_{SL} and H_{FL} in Pt/CoFe/MgO (**e**) and Ta/CoFe/MgO (**f**), when the magnetization is up and the electron flow is in the $+x$ direction.

orientation (Fig. 3c,d). The magnitude of H_{FL} in Pt/CoFe/MgO (Fig. 3c) was ≈20 Oe per 10^{11} A m^{-2}, two orders of magnitude lower than reported in refs 17,22, although its directionality was the same as in Pt/Co/AlOx (refs 17,22). As current-induced DW motion had a very high efficiency and occurred against the electron flow direction in Pt/CoFe/MgO, the fact that H_{FL} was negligible indicates

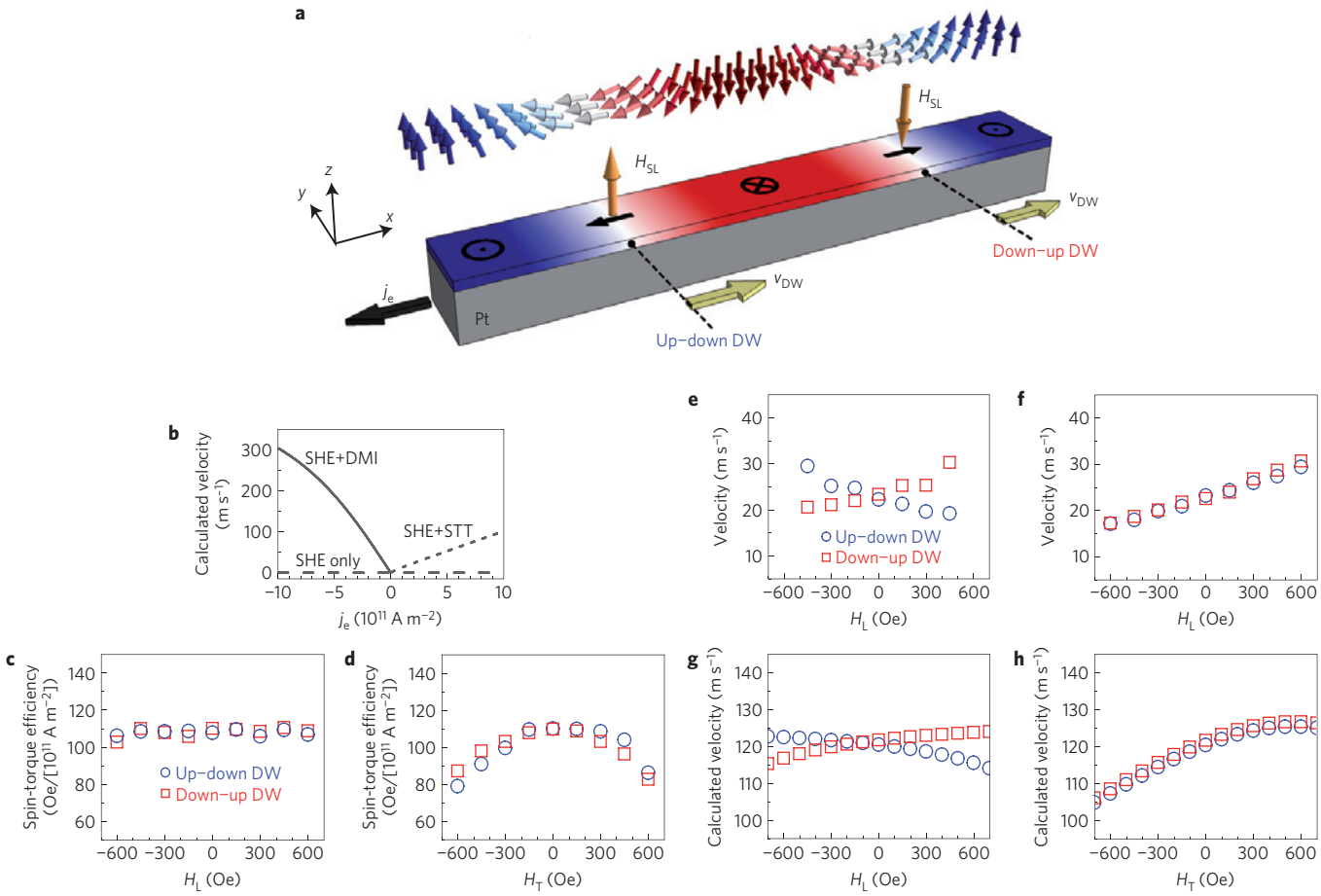

Figure 4 | Current-driven dynamics of chiral Néel DWs. a, Illustration of left-handed chiral Néel DWs in Pt/CoFe/MgO. The effective field H_{SL} from the Slonczewski-like torque moves adjacent up–down and down–up domains with velocity v_{DW} in the same direction against electron flow j_e. **b**, DW velocity as a function of electron current density j_e, calculated using the 1D model, with the SHE alone, the SHE and STT (SHE+STT), and the SHE and the DMI (SHE+DMI). The parameters used in this calculation are in the Methods. **c**,**d**, Spin-torque efficiency for DW motion in Pt/CoFe/MgO under applied longitudinal field H_L (**c**) and transverse field H_T (**d**). **e**,**f**, DW velocity at a constant current $j_e = -3.0 \times 10^{11}$ A m^{-2} as a function of H_L (**e**) and H_T (**f**). **g**,**h**, Calculated DW velocity at $j_e = -3.0 \times 10^{11}$ A m^{-2} as a function of H_L (**g**) and H_T (**h**) using the 1D model.

that the Rashba effect cannot be the source of these features[8–11,26,27]. Furthermore, as any contribution to the Slonczewski-like torque by the Rashba effect[18] enters as a correction proportional to the non-adiabicity parameter $\beta < 1$ (refs 26,27), the fact that H_{SL} is here much larger than H_{FL} implies that the Rashba effect contributes negligibly to the Slonczewski-like torque.

In Ta/CoFe/MgO (Fig. 3d), H_{FL} was in contrast quite large, ≈400 Oe per 10^{11} A m^{-2}, and its direction was the same as in Ta/CoFeB/MgO (ref. 23) and opposite to Pt/CoFe/MgO and Pt/Co/AlOx (refs 17,22). This result suggests that in addition to the Slonczewski-like torque, a strong Rashba field[17,22,23] may exist in this sample. However, the origin of the measured H_{FL} is beyond the scope of the present discussion and will require further investigation.

As summarized in Fig. 3e,f, the current-induced torques are opposite in Pt/CoFe/MgO and Ta/CoFe/MgO, as are the direction of current-driven DW motion and the sign of the spin Hall angles in Pt and Ta. Here we consider in detail the case of Pt/CoFe/MgO, in which the field-like torque is unambiguously small. One-dimensional (1D) model calculations[29] in Fig. 4b (see Methods and Supplementary Information) show that Bloch DWs cannot be driven by the SHE alone, in agreement with previous reports[16,27] and with the symmetry of the Slonczewski-like torque. In the 1D model with $\theta_{SH} > 0$ and with no transverse Rashba field, the addition of conventional STT enables sustained DW motion, but its direction is along electron flow (Fig. 4b). No combination of the SHE and STT reproduces the experimentally observed DW motion against electron flow (Supplementary Information), and moreover conventional STT is probably absent as argued above. Thus, an alternative mechanism is required whereby the SHE alone can drive DW motion.

Néel DWs have an internal magnetization that would align with the nanowire axis, such that the Slonczewski-like torque would manifest as a z-axis field[16] as experimentally observed (Fig. 1). However, the direction of H_{SL} depends of the sense of the DW magnetization, and the direction of DW motion varies accordingly (Supplementary Information). Figure 4a illustrates Néel DWs with oppositely directed internal magnetization for up–down and down–up transitions, exhibiting a left-handed chiral texture[2]. On the basis of the sign of the measured Slonczewski-like torque (Figs 2 and 3), these chiral DWs move against electron flow in Pt/CoFe/MgO and along electron flow in Ta/CoFe/MgO. Although Bloch DWs are magnetostatically preferred[28], adding the DMI to the 1D model stabilizes such chiral Néel DWs (ref. 7; Methods and Supplementary Information), leading to qualitative behaviour in agreement with experiment (Fig. 4b).

Finally, we assess the rigidity and chirality of the Néel DWs in Pt/CoFe/MgO using applied in-plane fields. In Fig. 4c,d we show that the spin-torque efficiency, extracted similarly to Fig. 1d, is insensitive to H_L up to at least 600 Oe, but declines significantly

with increasing $|H_T|$. This behaviour is opposite to that reported for Bloch DWs in ref. 15, but is precisely what is expected for DMI-stabilized Néel DWs: H_L is collinear with the DW magnetization and exerts no torque, whereas H_T exerts a torque that cants the DW magnetization away from the x axis and reduces the z-axis-oriented H_{SL}. That the sense of internal DW magnetization could not be reversed at the experimentally available maximum H_L of 600 Oe attests to the strength of the DMI in this system.

We also measured the effects of H_L and H_T on the velocity of fast current-driven DWs (Fig. 4e,f), which was reproduced qualitatively by the 1D model with the SHE and DMI (Fig. 4g,h). H_L modified the velocities of up–down and down–up DWs with opposite slopes (Fig. 4e,g), whereas H_T modified both velocities identically (Fig. 4f,h). The 1D model predicts DW motion reversal under very large H_L coinciding with reversal of the DW sense, and impeded motion for large H_T due to rotation towards a Bloch configuration (see Supplementary Information). Interestingly, the velocity increased with H_T in the direction of the previously reported Rashba field in Pt/Co/AlOx (refs 10,17,22), although here H_{FL} in Pt/CoFe/MgO was vanishingly small. Our experimental and computational results indicate that, even without the Rashba effect, H_T can modify the dynamics of Néel DWs driven by the SHE-induced Slonczewski-like torque. Although quantitative discrepancies exist between the 1D model calculations and the experimental results, the qualitative features based on the symmetries of the current-induced torques and DMI agree well with the experimental results.

We show that current alone drives DWs in Pt/CoFe/MgO and Ta/CoFe/MgO with high efficiency but in opposite directions, through the Slonczewski-like torque due to the SHE (refs 12–15). However, the SHE-induced torque alone cannot directly drive the magnetostatically preferred Bloch DWs (ref. 28) in these materials. We show experimentally and computationally that the DMI (refs 1–7) provides the missing ingredient to explain current-induced DW motion in heavy-metal/ferromagnet/oxide systems[8–11] by stabilizing Néel DWs with a built-in chirality, such that the SHE alone drives them uniformly and with high efficiency. Engineering both the DW spin structure and the current-induced torque simply by selecting the materials adjacent to the ferromagnet presents unprecedented opportunities for designing current-controlled spintronic devices.

Methods

Sample fabrication. The stack structure of Pt/CoFe/MgO was Ta(3 nm)/Pt(3 nm)/$Co_{80}Fe_{20}$(0.6 nm)/MgO(1.8 nm)/Ta(2 nm), and that of Ta/CoFe/MgO was Ta(5 nm)/$Co_{80}Fe_{20}$(0.6 nm)/MgO(1.8 nm)/Ta(2 nm). Both were deposited on Si/SiO_2(50 nm) substrates. The metal layers were deposited by d.c. magnetron sputtering at 2 mtorr Ar (for Pt, 3 mtorr Ar), and MgO was radiofrequency sputtered at 3 mtorr Ar. The deposition rates were <0.1 nm s^{-1}, calibrated with X-ray reflectivity. $Co_{80}Fe_{20}$ was chosen, instead of pure Co, to attain sufficient perpendicular magnetic anisotropy on both Ta and Pt underlayers. The bottom Ta(3 nm) layer in Pt/CoFe/MgO served as a seed layer to enhance perpendicular magnetic anisotropy and adhesion between Pt and the substrate. The Ta(2 nm) capping layer protected the MgO layer in each structure. Vibrating sample magnetometry on continuous films revealed full out-of-plane remanent magnetization and in-plane (hard axis) saturation fields of ≈5 kOe for Pt/CoFe/MgO and ≈3 kOe for Ta/CoFe/MgO. The saturation magnetization was ≈700 e.m.u. cm^{-3}, approximately half of the bulk value, suggesting a magnetic dead layer due to roughness or oxidation. Both films exhibited weak DW pinning, with DW propagation at fields <20 Oe.

The nanowires and Hall crosses were fabricated using electron beam lithography, magnetron sputtering and liftoff. Electrical contacts consisting of Ta(2 nm)/Cu(100 nm) were placed with a second layer of electron beam lithography. To estimate the current density through these devices, current was assumed to flow only through the ultrathin CoFe layer and the adjacent heavy metal layer, so that the effective conductive thickness was 3.6 nm for Pt/CoFe/MgO and 5.6 nm for Ta/CoFe/MgO. We neglected current shunting in the bottom Ta seed layer in the Pt/CoFe/MgO, as sputtered Ta (beta phase) typically has a much higher resistivity than Pt. The resistance of the Ta/CoFe/MgO device was 3.5 times greater than the Pt/CoFe/MgO device, and the Ta layer was estimated to be 5 times more resistive than the Pt layer. Current shunting through the Ta capping layer, assumed to be oxidized, was also neglected.

1D model. The DW velocity was calculated using the 1D model[29], which describes the DW in terms of two collective coordinates: position $X(t)$ and angle $\Phi(t)$, defined as the in-plane (x–y) angle with respect to the positive x axis. The current $\mathbf{j}_a = j_a\hat{x}$ is injected along the x axis, and is positive along the positive x axis. (Note that the electron flow j_e in the text is in the opposite direction with respect to j_a.) The 1D model including adiabatic and non-adiabatic STT, Slonczewski-like torque from the SHE, and the DMI (ref. 7) is given by

$$(1+\alpha^2)\frac{dX}{dt} = \alpha\gamma_0\Delta H_z - \frac{\gamma_0\Delta H_K}{2}\sin(2\Phi) + (1+\alpha\beta)b_J + \alpha\gamma_0\Delta\frac{\pi}{2}H_{SHE}\cos(\Phi) + \gamma_0\Delta\frac{\pi}{2}H_{DMI}\sin(\Phi) - \gamma_0\Delta\frac{\pi}{2}H_y\cos(\Phi) + \gamma_0\Delta\frac{\pi}{2}H_x\sin(\Phi)$$

and

$$(1+\alpha^2)\frac{d\Phi}{dt} = \gamma_0 H_z + \alpha\frac{\gamma_0 H_K}{2}\sin(2\Phi) + (\beta-\alpha)\frac{b_J}{\Delta} + \gamma_0\frac{\pi}{2}H_{SHE}\cos(\Phi) - \alpha\gamma_0\frac{\pi}{2}H_{DMI}\sin(\Phi) + \alpha\gamma_0\frac{\pi}{2}H_y\cos(\Phi) - \alpha\gamma_0\frac{\pi}{2}H_x\sin(\Phi)$$

where Δ is the DW width, H_K is the shape anisotropy field, α is the Gilbert damping, γ_0 is the gyromagnetic ratio, and b_J is related to the adiabatic STT, and is given by

$$b_J = \frac{\mu_B P}{eM_s}j_a$$

and β is the non-adiabatic parameter. Here, P is the spin polarization of the current, $\mu_B = 9.274\times10^{-24}$ J T^{-1} is the Bohr magneton, $e = -1.6\times10^{-19}$ C is the electron charge and M_S is the saturation magnetization. The applied magnetic field has components (H_x, H_y, H_z). The Slonczewski-like torque from the SHE enters the 1D model equations through the effective field parameter

$$H_{SHE} = \frac{\hbar\theta_{SH}j_a}{2\mu_0 eM_s t_F}$$

where θ_{SH} is the spin Hall angle and t_F is the thickness of the ferromagnetic layer. The effective field describing the DMI is[7]

$$H_{DMI} = \frac{D}{\mu_0 M_s\Delta}$$

where D is the DMI parameter. In the 1D model, the DMI enters as an effective field directed along the x axis inside the DW (ref. 7), and promotes Néel DWs with internal magnetization oriented in either direction along the x axis depending on the sign of D. The same chirality is therefore introduced for up–down and down–up DWs by using D with opposite signs.

To qualitatively understand the experimental observations, archetypal parameters of a high perpendicular magnetic anisotropy sample, with its easy axis along the z axis, were considered: saturation magnetization $M_s = 3\times10^5$ A m^{-1}, exchange constant $A = 10^{-11}$ J m^{-1}, uniaxial anisotropy constant $K_u = 2\times10^5$ J m^{-3}, Gilbert damping $\alpha = 0.2$, spin polarization $P = 0.5$, non-adiabatic parameter $\beta = 0.4$, spin Hall angle $\theta_{SH} = 0.1$, and Dzyaloshinskii–Moriya constant $|D| = 0.5$ mJ m^{-2}. The 1D model inputs were chosen to be $\Delta = 8.32$ nm and $H_K = 12,533$ A m^{-1}, which correspond to a ferromagnetic strip of rectangular cross-section $L_y\times L_z = 120$ nm $\times$ 3 nm explored in detail in ref. 29. For these parameters and dimensions the static DW configuration in the absence of DMI was a Bloch DW magnetized along the y axis, which was the initial DW configuration. Further details and model results are described in the Supplementary Information.

Received 9 February 2013; accepted 1 May 2013; published online 16 June 2013

References

1. Bode, M. *et al.* Chiral magnetic order at surfaces driven by inversion asymmetry. *Nature* **447,** 190–193 (2007).
2. Heide, M., Bihlmayer, G. & Blügel, S. Dzyaloshinskii–Moriya interaction accounting for the orientation of magnetic domains in ultrathin films: Fe/W(110). *Phys. Rev. B* **78,** 140403 (2008).
3. Yu, X. Z. *et al.* Real-space observation of a two-dimensional skyrmion crystal. *Nature* **465,** 901–904 (2010).
4. Heinze, S. *et al.* Spontaneous atomic-scale magnetic skyrmion lattice in two dimensions. *Nature Phys.* **7,** 713–718 (2011).

5. Huang, S. X. & Chien, C. L. Extended skyrmion phase in epitaxial FeGe(111) thin films. *Phys. Rev. Lett.* **108,** 267201 (2012).
6. Moriya, T. New mechanism of anisotropic superexchange interaction. *Phys. Rev. Lett.* **4,** 228–230 (1960).
7. Thiaville, A., Rohart, S., Jué, É., Cros, V. & Fert, A. Dynamics of Dzyaloshinskii domain walls in ultrathin magnetic films. *Europhys. Lett.* **100,** 57002 (2012).
8. Moore, T. A. *et al.* High domain wall velocities induced by current in ultrathin Pt/Co/AlOx wires with perpendicular magnetic anisotropy. *Appl. Phys. Lett.* **93,** 262504 (2008).
9. Miron, I. M. *et al.* Domain wall spin torquemeter. *Phys. Rev. Lett.* **102,** 137202 (2009).
10. Miron, I. M. *et al.* Fast current-induced domain-wall motion controlled by the Rashba effect. *Nature Mater.* **10,** 419–423 (2011).
11. Emori, S., Bono, D. C. & Beach, G. S. D. Interfacial current-induced torques in Pt/Co/GdOx. *Appl. Phys. Lett.* **101,** 042405 (2012).
12. Liu, L., Lee, O. J., Gudmundsen, T. J., Ralph, D. C. & Buhrman, R. A. Current-induced switching of perpendicularly magnetized magnetic layers using spin torque from the spin Hall effect. *Phys. Rev. Lett.* **109,** 096602 (2012).
13. Liu, L. *et al.* Spin-torque switching with the giant spin Hall effect of tantalum. *Science* **336,** 555–558 (2012).
14. Pai, C-F. *et al.* Spin transfer torque devices using the giant spin Hall effect of tungsten. *Appl. Phys. Lett.* **101,** 122404 (2012).
15. Haazen, P. P. J. *et al.* Domain wall depinning governed by the spin Hall effect. *Nature Mater.* **12,** 299–303 (2013).
16. Khvalkovskiy, A. V. *et al.* Matching domain-wall configuration and spin–orbit torques for efficient domain-wall motion. *Phys. Rev. B* **87,** 020402 (2013).
17. Miron, I. M. *et al.* Current-driven spin torque induced by the Rashba effect in a ferromagnetic metal layer. *Nature Mater.* **9,** 230–234 (2010).
18. Miron, I. M. *et al.* Perpendicular switching of a single ferromagnetic layer induced by in-plane current injection. *Nature* **476,** 189–193 (2011).
19. Parkin, S. S. P., Hayashi, M. & Thomas, L. Magnetic domain-wall racetrack memory. *Science* **320,** 190–194 (2008).
20. Allwood, D. A. *et al.* Magnetic domain-wall logic. *Science* **309,** 1688–1692 (2005).
21. Currivan, J., Jang, Y., Mascaro, M. D., Baldo, M. A. & Ross, C. A. Low energy magnetic domain wall Logic in short, narrow, ferromagnetic wires. *IEEE Magn. Lett.* **3,** 3000104 (2012).
22. Pi, U. H. *et al.* Tilting of the spin orientation induced by Rashba effect in ferromagnetic metal layer. *Appl. Phys. Lett.* **97,** 162507 (2010).
23. Suzuki, T. *et al.* Current-induced effective field in perpendicularly magnetized Ta/CoFeB/MgO wire. *Appl. Phys. Lett.* **98,** 142505 (2011).
24. Thiaville, A., Nakatani, Y., Miltat, J. & Suzuki, Y. Micromagnetic understanding of current-driven domain wall motion in patterned nanowires. *Europhys. Lett.* **69,** 990–996 (2005).
25. Cormier, M. *et al.* Effect of electrical current pulses on domain walls in Pt/Co/Pt nanotracks with out-of-plane anisotropy: Spin transfer torque versus Joule heating. *Phys. Rev. B* **81,** 024407 (2010).
26. Wang, X. & Manchon, A. diffusive spin dynamics in ferromagnetic thin films with a Rashba interaction. *Phys. Rev. Lett.* **108,** 117201 (2012).
27. Kim, K-W., Seo, S-M., Ryu, J., Lee, K-J. & Lee, H-W. Magnetization dynamics induced by in-plane currents in ultrathin magnetic nanostructures with Rashba spin–orbit coupling. *Phys. Rev. B* **85,** 180404 (2012).
28. Koyama, T. *et al.* Observation of the intrinsic pinning of a magnetic domain wall in a ferromagnetic nanowire. *Nature Mater.* **10,** 194–197 (2011).
29. Martinez, E. The stochastic nature of the domain wall motion along high perpendicular anisotropy strips with surface roughness. *J. Phys. Condens. Matter* **24,** 024206 (2012).
30. Kim, J. *et al.* Layer thickness dependence of the current-induced effective field vector in Ta|CoFeB|MgO. *Nature Mater.* **12,** 240–245 (2012).

Acknowledgements

This work was supported in part by the National Science Foundation under NSF-ECCS-1128439. Technical support from D. Bono is gratefully acknowledged. Devices were fabricated using instruments in the MIT Nanostructures Laboratory, the Scanning Electron-Beam Lithography facility at the Research Laboratory of Electronics, and the Center for Materials Science and Engineering at MIT. S.E. acknowledges financial support by the NSF Graduate Research Fellowship Program. The work by E.M. was supported by projects MAT2011-28532-C03-01 from the Spanish government and SA163A12 from Junta de Castilla y Leon.

Author contributions

G.S.D.B. proposed and supervised the study. S.E. and G.S.D.B. designed the experiments. S.E. and U.B. built the measurement set-ups with assistance from G.S.D.B. S-M.A. developed and deposited the Ta/CoFe/MgO and Pt/CoFe/MgO films. S.E. carried out the lithographic steps and performed all measurements. E.M. performed the modelling and wrote the corresponding text. S.E. analysed the data. S.E. and G.S.D.B. wrote the manuscript with assistance from U.B. All authors discussed the results and commented on the manuscript.

Additional information

Supplementary information is available in the online version of the paper. Reprints and permissions information is available online at www.nature.com/reprints. Correspondence and requests for materials should be addressed to G.S.D.B.

Competing financial interests

The authors declare no competing financial interests.